J|A|C|S ARTICLES

Published on Web 07/01/2009

Direct Observation of Lanthanide(III)-Phthalocyanine Molecules on Au(111) by Using Scanning Tunneling Microscopy and Scanning Tunneling Spectroscopy and Thin-Film Field-Effect Transistor Properties of Tb(III)- and Dy(III)-Phthalocyanine Molecules

Keiichi Katoh,[†] Yusuke Yoshida,[†] Masahiro Yamashita,*[,†] Hitoshi Miyasaka,[†] Brian K. Breedlove,[†] Takashi Kajiwara,[†] Shinya Takaishi,[†] Naoto Ishikawa,[‡] Hironari Isshiki,[§] Yan Feng Zhang,[§] Tadahiro Komeda,*[,§] Masakazu Yamagishi,[$] and Jun Takeya[$]

Department of Chemistry, Graduate School of Science, Tohoku University, Aramaki-Aza-Aoba, Aoba-Ku, Sendai 980-8578, Japan, Institute of Multidisciplinary Research for Advanced Materials (IMRAM), Tohoku University, 2-1-1, Katahira, Aoba-Ku, Sendai, 980-0877, Japan, Department of Chemistry, Chuo University, 1-13-27 Kasuga, Bunkyo-Ku, Tokyo 112-8551, Japan, and Department of Chemistry, Graduate School of Science, Osaka University, 1-1 Machikaneyama-Cho, Toyonaka, Osaka 560-0043, Japan

Received March 25, 2009; E-mail: yamasita@agnus.chem.tohoku.ac.jp

Abstract: The crystal structures of double-decker single molecule magnets (SMM) $LnPc_2$ (Ln = Tb(III) and Dy(III); Pc = phthalocyanine) and non-SMM YPc_2 were determined by using X-ray diffraction analysis. The compounds are isomorphous to each other. The compounds have metal centers (M = Tb^{3+}, Dy^{3+}, and Y^{3+}) sandwiched by two Pc ligands via eight isoindole-nitrogen atoms in a square-antiprism fashion. The twist angle between the two Pc ligands is 41.4°. Scanning tunneling microscopy was used to investigate the compounds adsorbed on a Au(111) surface, deposited by using the thermal evaporation in ultrahigh vacuum. Both MPc_2 with eight lobes and MPc with four lobes, which has lost one Pc ligand, were observed. In the scanning tunneling spectroscopy images of TbPc molecules at 4.8 K, a Kondo peak with a Kondo temperature (T_K) of ~250 K was observed near the Fermi level ($V = 0$ V). On the other hand, DyPc, YPc, and MPc_2 exhibited no Kondo peak. To understand the observed Kondo effect, the energy splitting of sublevels in a crystal field should be taken into consideration. As the next step in our studies on the SMM/Kondo effect in Tb-Pc derivatives, we investigated the electronic transport properties of Ln-Pc molecules as the active layer in top- and bottom-contact thin-film organic field effect transistor devices. Tb-Pc molecule devices exhibit *p*-type semiconducting properties with a hole mobility (μ_H) of $\sim 10^{-4}$ cm^2 V^{-1} s^{-1}. Interestingly, the Dy-Pc based devices exhibited ambipolar semiconducting properties with an electron mobility (μ_e) of $\sim 10^{-5}$ and a μ_H of $\sim 10^{-4}$ cm^2 V^{-1} s^{-1}. This behavior has important implications for the electronic structure of the molecules.

Introduction

Accessing data on the nanolevel is extremely important in nanoscience and nanotechnology.[1,2] Experiments have been performed on single molecules,[3] nanotubes,[4] and quantum dots[5] on metallic electrodes via tunnel barriers, which have given rise to the idea of energy-level quantization dominated electron transportation.

The idea of using a single spin as a "bit" of information to prepare high-density storage and quantum computing devices has caused an increase in scientific and technological interests. The underlying phenomenon for this idea is quantum tunneling magnetization (QTM) between double well potentials,[6] which is a prominent characteristic property of single molecule magnets (SMMs).[7] Tremendous efforts have been devoted to creating

[†] Tohoku University.
[‡] Chuo University.
[§] IMRAM, Tohoku University.
[$] Osaka University.

(1) Aviram, A.; Ratner, M. A. *Chem Phys lett.* **1974**, *29*, 277–283.
(2) Kuhn, H.; Mobius, D. *Angew. Chem., Int. Ed. Engl.* **1971**, *10*, 620–637.
(3) (a) Xu, B.; Tao, N. J. *Science* **2003**, *301*, 1221–1223. (b) Galperin, M.; Ratner, M. A.; Nitzan, A.; Troisi, A. *Science* **2008**, *319*, 1056–1060. (c) Haiss, W.; Wang, C.; Grace, I.; Batsanov, A. S.; Schiffrin, D. J.; Higgins, S. J.; Bryce, M. R.; Lambert, C. J.; Nichols, R. J. *Nat. Mater.* **2006**, *5*, 995–1002.
(4) LeMieux, M. C.; Roberts, M.; Barman, S.; Jin, Y. W.; Kim, J. M.; Bao, Z. *Science* **2008**, *321*, 101–104.
(5) (a) Goldhaber-Gordon, D.; Shtrikman, H.; Mahalu, D.; Abusch-Magder, D.; Meirav, U.; Kastner, M. A. *Nature* **1998**, *391*, 156–159. (b) Jeong, H.; Chang, A. M.; Melloch, M. R. *Science* **2001**, *293*, 2221–2223. (c) Ng, T. K.; Lee, P. A. *Phys. Rev. Lett.* **1988**, *61*, 1768–1771.
(6) Gatteschi, D.; Sessoli, R.; Villain, J. *Molecular Nanomagnets*; Oxford University Press: New York, 2007.
(7) (a) Krusin-Elbaum, L.; Shibauchi, T.; Argyle, B.; Gignac, L.; Weller, D. *Nature* **2001**, *410*, 444–446. (b) Bogani, L.; Wernsdorfer, W. *Nat. Mater.* **2008**, *7*, 179–186.

memory and spintronic devices by designing the molecular and/or crystal structure and isolating the SMMs. Studies involving $[Mn_{12}O_{12}(O_2CR)_{16}(H_2O)_4]$ under single-molecule transistor operating conditions have resulted in the discovery of new electronic transport phenomena, such as negative differential conductance and complete current suppression.[8] The latter phenomenon occurs below a blocking temperature (T_B) of 4−6 K, in relation to an energy scale that corresponds to an anisotropy barrier.

At the same time, researchers have been studying compounds with a T_B higher than that of the Mn cluster.[8] Recently, Ishikawa et al.[9] have reported that double-decker phthalocyaninato lanthanide molecules $TBA^+[TbPc_2]^-$ ($TBA^+ = (C_4H_9)_4N^+$, Pc = dianion of phthalocyanine) have a long magnetization relaxation time as an intrinsic molecular property and can function as SMMs. Lanthanide(III)-Pc molecules showing SMM behavior have significantly large axial magnetic anisotropies, which occur by a different mechanism than those for known 3d metal cluster SMMs.[8] In the case of 3d cluster SMMs, an easy axis-type magnetic anisotropy, which is represented by the negative zero-field splitting constant (D), is caused by the magnetic interactions among high-spin 3d metal ions in the cluster. In the case of lanthanide SMMs, on the other hand, the ligand field of the lanthanide ion controls the anisotropy. The ligand field potential around the Tb^{3+} ion ($4f^8$) with a total angular momentum (J) of 6 splits the ground multiplet so that the lowest sublevel has the largest J_z value ($|J_z| = 6$, corresponding to up/down spin states) and large energy gaps to the remaining sublevels (ca. 400 cm^{-1}).[9] Because of this unusual condition, there is a small probability for a transition between $J_z = 6$ (up-spin state) and -6 (down-spin state) substates and hence a slow magnetization response to an applied magnetic field. In alternating current (ac) magnetic susceptibility measurements, $[TbPc_2]^-$ exhibits a characteristic peak in a χ_M'' versus T plot (χ_M'' refers to the out-of-phase component of the ac molar susceptibility) at 40 K in an ac magnetic field of 997 Hz. However, there have been no reports of transition-metal-cluster SMMs showing a χ_M'' peak at higher than 7 K. The ligand field splitting pattern causes long magnetic relaxation times (0.1 ms to 1 s) at considerably high temperatures (<40 K).[9]

The anion $[LnPc_2]^-$ consists of a positive trivalent lanthanide ion and two Pc ligands, each having a formal charge of -2 with a closed shell π electron system. It is known that one-electron oxidation of $[LnPc_2]^-$ occurs at the ligand, resulting in the neutral $[LnPc_2]^0$ with an open shell π electron system.[10] The $TbPc_2$ molecule therefore has two spin systems, i.e., an unpaired π electron on the Pc ligands and a Tb^{3+} ion with 4f electrons. Alternating current magnetic susceptibility measurements on $TbPc_2$ have shown that oxidation of Pc ligands in $[TbPc_2]^-$ causes a significant upward shift in the temperature range where the magnetization response shows a phase lag behind the time-varying external magnetic field. Peaks for χ_M'' of the π-radical $TbPc_2$ have been observed at 50, 43, and 36 K with ac magnetic fields of 10^3, 10^2, and 10 Hz, respectively, which are more than 10 K higher than the corresponding values of the anionic complex with a closed-shell π-system.[9] To investigate the stability of a vacuum and evaporation method and the magnetic anisotropy in a specific direction after transferring to a surface, Vitali et al. have recently reported the electronic structure (SMM character) of $TbPc_2$ deposited on a Cu(111) surface in an ultrahigh vacuum (UHV) using a dry imprint technique.[11] On the basis of the properties of $LnPc_2$ SMMs, we think that $TbPc_2$ can be used as a "bit" of information in high density storage technology by taking advantage of the single up-spin/down-spin property.

$TbPc_2$ SMMs may couple with magnetic impurities including Tb^{3+} ions and/or conducting electrons from the tunneling current in scanning tunneling spectroscopy (STS). This phenomenon is known as the Kondo effect.[12] The magnetic properties of transition metal atoms in a host molecule can be elucidated via the Kondo resonance in cryogenic scanning tunneling microscopy (STM).[13−15] Most of the previous studies on the Kondo effect have focused on magnetic atoms on open metal surfaces.[16] However, the Kondo temperature (T_K) in these systems is very low, and the spin-dependent transport properties are consequently lost under ambient conditions. Recent studies on molecular Kondo effects show that caging the magnetic atoms

(8) (a) Cornia, A.; Costantino, A. F.; Zobbi, L.; Caneschi, A.; Gatteschi, D.; Mannini, M.; Sessoli, R. *Struct. Bonding (Berlin)* **2006**, *122*, 133–161. (b) Fleury, B.; Catala, L.; Huc, V.; David, C.; Zhong, W. Z.; Jegou, P.; Baraton, L.; Palacin, S.; Albouy, P.-A.; Mallah, T. *Chem. Commun.* **2005**, 2020–2022. (c) Naitabdi, A.; Bucher, J.-P.; Gerbier, Ph.; Rabu, P.; Drillon, M. *Adv. Mater.* **2005**, *17*, 1612–1616. (d) Heersche, H. B.; de Groot, Z.; Folk, J. A.; van der Zant, H. S. J.; Romeike, C.; Wegewijs, M. R.; Zobbi, L.; Barreca, D.; Tondello, E.; Cornia, A. *Phys. Rev. Lett.* **2006**, *96*, 206801–206804. (e) Jo, M.-H.; Grose, J. E.; Baheti, K.; Deshmukh, M. M.; Sokol, J. J.; Rumberger, E. M.; Hendrickson, D. N.; Long, J. R.; Park, H.; Ralph, D. C. *Nano. Lett.* **2006**, *6*, 2014–2020.

(9) (a) Ishikawa, N.; Sugita, M.; Ishikawa, T.; Koshihara, S.; Kaizu, Y. *J. Am. Chem. Soc.* **2003**, *125*, 8694–8695. (b) Ishikawa, N.; Sugita, M.; Ishikawa, T.; Koshihara, S.; Kaizu, Y. *J. Phys. Chem. B* **2004**, *108*, 11265–11271. (c) Ishikawa, N. *Polyhedron* **2007**, *26*, 2147–2153. (d) Takamatsu, S.; Ishikawa, T.; Koshihara, S.; Ishikawa, N. *Inorg. Chem.* **2007**, *46*, 7250–7252. (e) Takamatsu, S.; Ishikawa, N. *Polyhedron* **2007**, *26*, 1859–1862. (f) Ishikawa, N.; Sugita, M.; Wernsdorfer, W. *Angew. Chem., Int. Ed.* **2005**, *44*, 2931–2935. (g) Ishikawa, N.; Sugita, M.; Wernsdorfer, W. *J. Am. Chem. Soc.* **2005**, *127*, 3650–3651. (h) Ishikawa, N.; Sugita, M.; Okubo, T.; Tanaka, N.; Iino, T.; Kaizu, Y. *Inorg. Chem.* **2003**, *42*, 2440–2446. (i) Ishikawa, N. *J. Phys. Chem. A* **2003**, *107*, 5831–5835. (j) Ishikawa, N.; Kaizu, Y. *Coord. Chem. Rev.* **2002**, *226*, 93–101.

(10) Ishikawa, N.; Sugita, M.; Tanaka, N.; Ishikawa, T.; Koshihara, S.; Kaizu, Y. *Inorg. Chem.* **2004**, *43*, 5498–5500.

(11) (a) Vitali, L.; Fabris, S.; Conte, A. M.; Brink, S.; Ruben, M.; Baroni, S.; Kern, K. *Nano Lett.* **2008**, *8*, 3364–3368. (b) Gómez-Segura, J.; Díez-Pérez, I.; Ishikawa, N.; Nakano, M.; Veciana, J.; Ruiz-Molina, D. *Chem. Commun.* **2006**, 2866–2868. (c) Zhang, Y. F.; Isshiki, H.; Katoh, K.; Yoshida, Y.; Yamashita, M.; Miyasaka, H.; Breedlove, B. K.; Kajiwara, T.; Takaishi, S.; Komeda, T. *J. Phys. Chem. C* **2009**, *113*, 9826–9830.

(12) Michael, N. *Nature* **2001**, *410*, 789–793.

(13) Iancu, V.; Deshpande, A.; Hla, S. W. *Nano Lett.* **2006**, *6*, 820–823.

(14) Wahl, P.; Diekhöner, L.; Wittich, G.; Vitali, L.; Schneider, M. A.; Kern, K. *Phys. Rev. Lett.* **2005**, *95*, 166601–166604.

(15) Zhao, A.; Li, Q.; Chen, L.; Xiang, H.; Wang, W.; Pan, S.; Wang, B.; Xiao, X.; Yang, J.; Hou, J. G.; Zhu, Q. *Science* **2005**, *309*, 1542–1544.

(16) (a) Madhavan, V.; Chen, W.; Jamneala, T.; Crommie, M. F.; Wingreen, N. S. *Science* **1998**, *280*, 567–569. (b) Manoharan, H. C.; Lutz, C. P.; Eigler, D. M. *Nature* **2000**, *403*, 512–515. (c) Knorr, N.; Schneider, M. A.; Diekhöner, L.; Wahl, P.; Kern, K. *Phys. Rev. Lett.* **2002**, *88*, 096804–096807. (d) Madhavan, V.; Jamneala, T.; Nagaoka, K.; Chen, W.; Li, J. L.; Louie, S. G.; Crommie, M. F. *Phys. Rev. B* **2002**, *66*, 212411–212414. (e) Chen, W.; Jamneala, T.; Madhavan, V.; Crommie, M. F. *Phys. Rev. B* **1999**, *60*, R8529–R8532. (f) Jamneala, T.; Madhavan, V.; Crommie, M. F. *Phys. Rev. Lett.* **2001**, *87*, 256804–256807. (g) Jamneala, T.; Madhavan, V.; Chen, W.; Crommie, M. F. *Phys. Rev. B* **2000**, *61*, 9990–9993. (h) Li, J.; Schneider, W.-D.; Berndt, R.; Delley, B. *Phys. Rev. Lett.* **1998**, *80*, 2893–2896. (i) Schneider, M. A.; Vitali, L.; Knorr, N.; Kern, K. *Phys. Rev. B* **2002**, *65*, 121406–121409. (j) Wahl, P.; Diekhöner, L.; Schneider, M. A.; Vitali, L.; Wittich, G.; Kern, K. *Phys. Rev. Lett.* **2004**, *93*, 176603–617660. (k) Nagaoka, K.; Jamneala, T.; Grobis, M.; Crommie, M. F. *Phys. Rev. Lett.* **2002**, *88*, 077205–077208. (l) Manoharan, H. C.; Lutz, C. P.; Eigler, D. M. *Nature* **2000**, *403*, 512–515.

in a molecule can increase[13,14,17] or decrease[15,17] T_K. In these cases, both the molecular structure[14,15] and the molecular conformation[13] play an important role. Among the studies, a report on the Kondo effect of single M-Pc molecules adsorbed on metal surfaces has attracted much attention.[15,18] This effect is a result of the exchange interaction between the local magnetic moment in the molecule and the conducting electrons. The properties of the M-Pc derivatives are important in the fabrication of single molecule devices.[19]

In relation to SMMs and the Kondo effect, organic field-effect transistors (OFETs), whose characteristics are modulated by an electrical field, are probably the most prominent constituent of next generation microelectronics.[20] They have attracted increasing interest especially for use in flexible and low-cost electronic applications, such as electronic paper, low-end display driving circuits, radio frequency identification tags, and smart cards.[21] Ambipolar OFETs are of particular interest because they can be operated in both *p*-channel and *n*-channel modes. This unique characteristic simplifies the preparation process when constructing complementary circuits.[22] Currently, most ambipolar OFETs are composed of layered or mixed films of *p*-type and *n*-type semiconducting molecules.[23] To act as ambipolar semiconductors for OFET applications, semiconductor molecules with large π-conjugated system should have (a) small ionization potentials and large electron affinities to achieve small injection barriers for both holes and electrons from a common Au source-drain electrode and (b) small reorganization energies and large transfer integrals to obtain large charge transfer mobility. M-Pc derivatives show ambipolar behavior in FET structures.[24] de Boer et al. have recently reported ambipolar OFETs with active layers composed of CuPc and FePc single crystals.[24c] Yasuda et al. have demonstrated ambipolar carrier transport in vapor-deposited CuPc OFETs with low work function Ca contacts, which reduce the electron injection barrier without breaking the vacuum.[24b] On the other hand, OFETs made from vapor-deposited CuPc with a hole mobility of $\sim 10^{-3}$ $cm^2\ V^{-1}\ s^{-1}$ (*p*-type behavior) under ambient conditions with oxygen acting as an acceptor and do not show *n*-type semiconduction.[25] An interesting correlation between the thin-film morphology (α-form), depending on the substrate deposition temperature, and the field-effect hole mobility has been reported.[25a−c]

This progress motivated us to investigate the unique electrical and magnetic properties of metal-Pc molecules by directly accessing the isolated molecules on a Au surface via scanning tunneling microscopy (STM) and scanning tunneling spectroscopy (STS) and to investigate the bulk phase electron transport properties for next generation devices. Here we describe the molecular structures and electronic transport properties of MPc_2 and MPc molecules (M = Tb^{3+}, Dy^{3+}, and Y^{3+}) on a Au(111) surface in relation to STS measurements using a cryogenic, ultrahigh vacuum (UHV) STM. We detected two types of molecules, and it is thought that one is a double-decker MPc_2 molecule (eight lobes)[11] and the other is the MPc molecule (four lobes), which formed as a result of the loss of a Pc. We observed a clear sharp feature near the Fermi level ($V = 0$ V) in the d*I*/d*V* spectra for TbPc, which was assigned to be a Kondo peak, similar to that in previously observed spectra for M-Pc molecules (CoPc,[15] FePc,[18] etc.). However, it could not be determined if there was a Kondo peak for DyPc and YPc. In addition, in order to study the electronic transport properties in the bulk phase, we fabricated thin-film OFETs with Tb-Pc and Dy-Pc molecular films as the active layers. Tb-Pc and Dy-Pc molecules exhibited *p*-type and ambipolar semiconductor properties, respectively. We think that the appearance of Kondo effect and FET properties is related to the electronic structures of the molecule, which were determined from the height of the barrier for spin relaxation determined from the splitting energy of the sublevels in the crystal field.

Experimental Section

Synthesis of MPc_2. All reagents were purchased from Wako or Aldrich and used without further purification. The compounds were prepared following a reported procedure with a slight modifica-

(17) Madhavan, V.; Chen, W.; Jamneala, T.; Crommie, M. F. *Phys. Rev. B* **2001**, *64*, 165412–165422.
(18) Gao, L.; Ji, W.; Hu, Y. B.; Cheng, Z. H.; Deng, Z. T.; Liu, Q.; Jiang, N.; Lin, X.; Guo, W.; Du, S. X.; Hofer, W. A.; Xie, X. C.; Gao, H.-J. *Phys. Rev. Lett.* **2007**, *99*, 106402–106405.
(19) (a) Park, J.; Pasupathy, A. N.; Goldsmith, J. I.; Chang, C.; Yaish, Y.; Petta, J. R.; Rinkoski, M.; Sethna, J. P.; Abruña, H. D.; McEuen, P. L.; Ralph, D. C. *Nature* **2002**, *417*, 722–725. (b) Liang, W.; Shores, M. P.; Bockrath, M.; Long, J. R.; Park, H. *Nature* **2002**, *417*, 725–729. (c) Yu, L. H.; Natelson, D. *Nano Lett.* **2004**, *4*, 79–83. (d) Yu, L. H.; Keane, Z. K.; Ciszek, J. W.; Cheng, L.; Stewart, M. P.; Tour, J. M.; Natelson, D. *Phys. Rev. Lett.* **2004**, *93*, 266802–266804. (e) Pasupathy, A. N.; Bialczak, R. C.; Martinek, J.; Grose, J. E.; Donev, L. A. K.; McEuen, P. L.; Ralph, D. C. *Science* **2004**, *306*, 86–89.
(20) Horowitz, G. *Adv. Mater.* **1998**, *10*, 365–377.
(21) (a) Sheraw, C. D.; Zhou, L.; Huang, J. R.; Gundlach, D. J.; Jackson, T. N.; Kane, M. G.; Hill, I. G.; Hammond, M. S.; Campi, J.; Greening, B. K.; Francl, J.; West, J. *Appl. Phys. Lett.* **2002**, *80*, 1088–1090. (b) Comiskey, B.; Albert, J. D.; Yoshizawa, H.; Jacobson, J. *Nature* **1998**, *394*, 253–255. (c) Crone, B.; Dodabalapur, A.; Gelperin, A.; Torsi, L.; Katz, H. E.; Lovinger, A. J.; Bao, Z. *Appl. Phys. Lett.* **2001**, *78*, 2229–2231. (d) Drury, C. J.; Mutsaers, C. M. J.; Hart, C. M.; Matters, M.; de Leeuw, D. M. *Appl. Phys. Lett.* **1998**, *73*, 108–110. (e) Gelinck, G. H.; Geuns, T. C. T.; de Leeuw, D. M. *Appl. Phys. Lett.* **2000**, *77*, 1487–1489. (f) Mach, P.; Rodriguez, S. J.; Nortrup, R.; Wiltzius, P.; Rogers, J. A. *Appl. Phys. Lett.* **2001**, *78*, 3592–3594. (g) Huitema, H. E. A.; Gelinck, G. H.; van der Putten, J. B. P. H.; Kuijk, K. E.; Hart, C.; Cantatore, E.; Herwigm, P. T.; van Breemen, A. J. J. M.; de Leeuw, D. M. *Nature* **2001**, *414*, 599. (h) Baude, P. F.; Ender, D. A.; Haase, M. A.; Kelley, T. W.; Muyres, D. V.; Thesis, S. D. *Appl. Phys. Lett.* **2003**, *82*, 3964–3966.
(22) (a) Dodabalapur, A.; Katz, H. E.; Torsi, L.; Haddon, R. C. *Science* **1995**, *269*, 1560–1562. (b) Meijer, E. J.; de Leeuw, D. M.; Setayesh, S.; van Veenendaal, E.; Huisman, B.-H.; Blom, P. W. M.; Hummelen, J. C.; Scherf, U.; Klapwijk, T. M. *Nat. Mater.* **2003**, *2*, 678–682.
(23) Rost, C.; Gundlach, D. J.; Karg, S.; Riess, W. *J. Appl. Phys.* **2004**, *95*, 5782–5787.
(24) (a) Tada, H.; Touda, H.; Takada, M.; Matsushige, K. *Appl. Phys. Lett.* **2000**, *76*, 873–875. (b) Yasuda, T.; Fujita, K.; Tsutsui, T. *Chem. Phys. Lett.* **2005**, *402*, 395–398. (c) de Boer, R. W. I.; Stassen, A. F.; Craciun, M. F.; Mulder, C. L.; Molinari, A.; Rogge, S.; Morpurgoa, A. F. *Appl. Phys. Lett.* **2005**, *86*, 262109–11. (d) Guillaud, G.; Sadoun, M. A.; Maitrot, M.; Simon, J.; Bouvet, M. *J. Chem. Phys. Lett.* **1990**, *167*, 503–506. (e) Su, W.; Jiang, J.; Xiao, K.; Chen, Y.; Zhao, Q.; Yu, G.; Liu, Y. *Langmuir* **2005**, *21*, 6527–6531. (f) Chen, Y.; Su, W.; Bai, M.; Jiang, J.; Li, X.; Liu, Y.; Wang, L.; Wang, S. *J. Am. Chem. Soc.* **2005**, *127*, 15700–15701. (g) Chen, Y.; Li, R.; Wang, R.; Ma, P.; Dong, S.; Gao, Y.; Li, X.; Jiang, J. *Langmuir* **2007**, *23*, 12549–12554. (h) Li, R.; Ma, P.; Dong, S.; Zhang, X.; Chen, Y.; Li, X.; Jiang, J. *Inorg. Chem.* **2007**, *46*, 11397–11404. (i) Zhang, Y.; Cai, X.; Qi, D.; Bian, Y.; Jiang, J. *J. Phys. Chem. C* **2008**, *112*, 14579–14588.
(25) (a) Bao, Z.; Lovinger, A. J.; Dodabalapur, A. *Appl. Phys. Lett.* **1996**, *69*, 3066–3068. (b) Hoshino, S.; Kamata, T.; Yase, K. *J. Appl. Phys.* **2002**, *92*, 6028–6032. (c) Xiao, K.; Liu, Y.; Yu, G.; Zhu, D. *Appl. Phys. A: Mater. Sci. Process.* **2003**, *77*, 367–369. (d) Xiao, K.; Liu, Y.; Yu, G.; Zhu, D. *Synth. Met.* **2003**, *137*, 991–992. (e) Yasuda, T.; Fujita, K.; Nakashima, H.; Tsutui, T. *Jpn. J. Appl. Phys.* **2003**, *42*, 6614–6618. (f) Sussman, A. *J. Appl. Phys.* **1967**, *38*, 2748–2752.
(26) (a) de Cian, A.; Moussavi, M.; Fischer, J.; Weiss, R. *Inorg. Chem.* **1985**, *24*, 3162–3167. (b) Paillaud, J. L.; Drillon, M.; Cian, A. D.; Fischer, J.; Weiss, R.; Villeneuve, G. *Phys. Rev. Lett.* **1991**, *67*, 244–247.

tion.[26] A mixture of 1,2-dicyanobenzene (62.7 mmol), $M(OAc)_3 \cdot 4H_2O$ (M = Tb^{3+}, Dy^{3+}, and Y^{3+}) (3.92 mmol), and 1,8-diazabicyclo[5,4,0]undec-7-ene (DBU) (33.5 mmol) in 200 mL of 1-hexanol was refluxed for 1.5 d. The solution was allowed to cool to room temperature and then filtered. The precipitate was washed with acetic anhydride, cold acetone, and *n*-pentane. Then, the precipitate was dried in air. The crude purple product was extracted with 10 × 200 mL portions of $CHCl_3$. The green extracts were combined, concentrated, and purified using column chromatography (C-200 silica gel, Wako). The eluent was 98:2 CH_2Cl_2/MeOH. The green fraction, which was also the first fraction, was collected with care not to contaminate with the anionic $[MPc_2]^{-1}$ complex, which was the second fraction (blue-green). The green fraction was concentrated, and *n*-hexane was added until the compound precipitated. The green precipitate was filtered and dried in vacuo. In general, the yield was 2−5%.

Deep green crystals of the products "without" CH_2Cl_2 were obtained by using a different solvent.[26] The green precipitate (8 mg) was dissolved in 20 mL of $CHCl_3$ and filtered. *n*-hexane was layered on the top of green filtrate. After 2 weeks, deep green needle-like crystals were obtained.

Measurements. Infrared spectra were recorded as KBr disks on a JASCO FT-IR 620 spectrometer at 298 K. UV−vis−NIR spectra of $CHCl_3$ solutions were measured in a quartz cell with a path length of 1 cm on a SHIMADZU UV-3100PC spectrometer at 298 K. Differential pulse voltammetry (DPV) and cyclic voltammetry (CV) were carried out on a Bioanalytical Systems, Inc. CV-50W version 2.0 for 10^{-3} mol L^{-1} solutions of the compounds in dry CH_2Cl_2 with *n*-Bu_4PF_6 (0.1 mol L^{-1}) as supporting electrolyte, using glass carbon working electrodes, Pt electrodes, and Ag/AgCl as the counter and reference electrodes; the following conditions were employed: scan rate = 50 mV s^{-1} for DPV and 100 mV s^{-1} for CV, pulse amplitude = 50 mV, pulse width = 50 ms, and pulse period = 0.1 s at 294 K. X-ray structure determination was as follows. A needle-like single crystal was mounted on the top of a glass tube with glue. All diffraction data were collected on a Rigaku CCD diffractometer (Saturn70) with graphite-monochromated Mo Kα radiation (λ = 0.7107 Å) at 93(1) K. All non-hydrogen atoms were refined anisotropically using a least-squares method, and hydrogen atoms were fixed at calculated positions and refined using a riding model. SHELXTL[27] was used for structure refinement.

Cryogenic STM measurements were performed in an UHV (2×10^{-8} Pa) at a sample temperature of 4.7 K. A commercially available STM head (U-999, Unisoku, Japan) was placed in a tube-like stainless chamber. The chamber was inserted into a He dewar and evacuated until a UHV was reached. The He dewar was attached to an air-suspended table and located below the floor level. The assembly of the tube scanner, STM tip, sample holder, and inertia slider for the coarse motion of the tip were suspended by springs to suppress vibrations. A bias voltage was applied to the sample. d*I*/d*V* spectra were measured using a lock-in technique with a modulation signal (4 mV, 487 Hz). The Au(111) surface was prepared in a UHV by repeated sputtering with Ar^+ and annealing at 900 K. M-Pc (M = Tb^{3+}, Dy^{3+}, and Y^{3+}) was deposited on the Au(111) surface by evaporation from a Ta boat heated at ∼600 K, after prolonged degassing of MPc_2 (M = Tb^{3+}, Dy^{3+}, and Y^{3+}) and the boat. X-ray photoemission spectroscopy (XPS) was executed by using nonmonochromatized Al Kα X-ray source (XSAM 800 pci, Kratos, U.K.).

Top- and bottom-contact devices were fabricated by evaporating $TbPc_2$ and $DyPc_2$ molecules (100 nm) on hexamethyldisilazane (HMDS, 500 nm) treated n^+-Si/SiO_2 substrates (see Figure S5, Supporting Information). Au (50 nm) was vacuum deposited for the source and drain electrodes. Length and width of the semiconductor channels of the OFET devices were 30 and 100 μm, respectively. FET characteristics were measured under ambient conditions using an Agilent 5207 Semiconductor Parameter Analyzer.

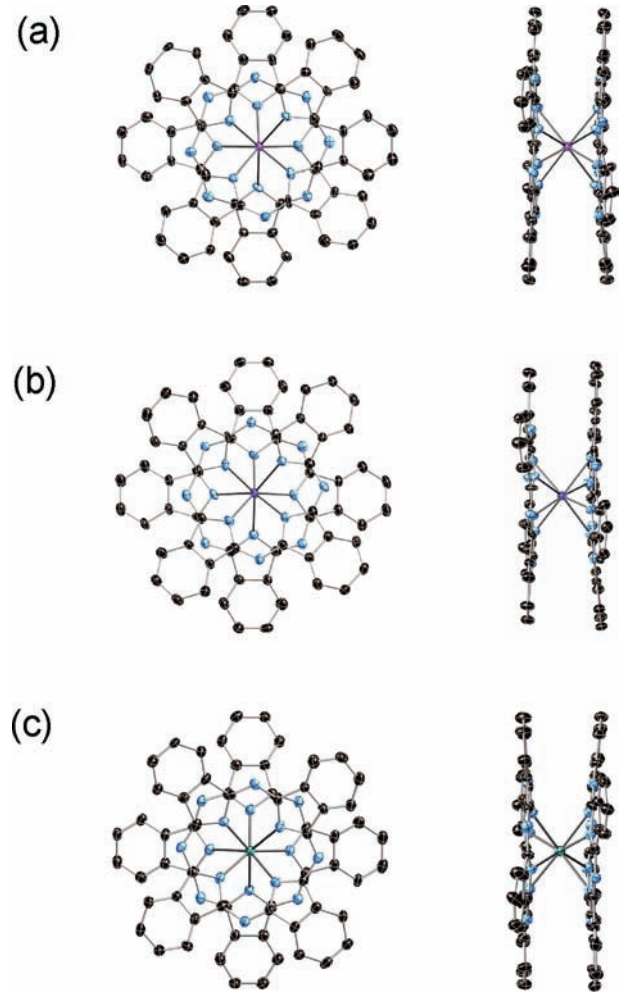

Figure 1. Crystal structures of (a) $TbPc_2$, (b) $DyPc_2$, and (c) YPc_2. Top view (left) and side view (right). The thermal ellipsoids are shown at the 50% probability for all non-hydrogen atoms.

Result and Discussion

Crystal and Electronic Structures of MPc_2. The MPc_2 (M = Tb^{3+}, Dy^{3+}, and Y^{3+}) molecules crystallized in the space group $P2_12_12_1$ (γ-phase) and were isomorphous with each other, as shown in Figure 1. The crystal data are summarized in Table S1, and crystals packing are shown in Figure S1, Supporting Information. Each complex has a metal ion sandwiched between two Pc with eight isoindole-nitrogen donor atoms. The eight M−N bond distances based on the ionic radius (r_{ion}) of the octa coordinate M(III) varied in the range of 0.240−0.243 nm for Tb^{3+} (r_{ion} = 0.118 nm), 0.239−0.242 nm for Dy^{3+} (r_{ion} = 0.117 nm), and 0.240−0.241 nm for Y^{3+} (r_{ion} = 0.116 nm). The twisted angle between the two rings was determined to be 41.4°, causing a pseudo 4-fold axis perpendicular to the Pc rings and a distorted antiprismatic coordination environment around the metal center. Both Pc rings are saucer-shaped and slightly distorted. However, one ring deviated more from planarity than the other. These crystal structures are similar to those of the previously described lanthanide Pc complexes with solvent molecules.[26] The size and height of this molecule were estimated to be ∼1.6 and ∼0.4 nm on the basis of the distance between the two hydrogen atoms at both ends and between the hydrogen

(27) Sheldrick, G. M. *SHELXTL, program for Crystal Structure Determination*; Siemens Analytical X-ray Instruments Inc.: Madison, WI, 1994.

atoms of the two Pc rings, respectively (structural details are Figure S1, Supporting Information).

The complexes had a one-electron ligand oxidized "sandwich" structure, in which the unpaired electron was delocalized on both phthalocyanine ligands.[28] Lanthanide double-decker Pc complexes generally exhibit two broad absorption bands characteristic of a radical Pc ligand in the 460−500 and 880−900 nm regions as well as another broadband in the range of 1200−1600 nm, corresponding to intramolecular charge transfer (ICT) between the two rings.[29] Therefore, near-IR spectroscopic studies were performed on three MPc_2 molecules in $CHCl_3$ (see Figure S2 and Table S2, Supporting Information). In this spectrum, only three main absorption bands in the UV−vis region were observed. The two absorption bands at 668 and 322 nm were assigned to the Q-band and Soret band, respectively. The weak shoulder attached to the Q-band (602 and 582 nm) has been reported to be due to the weak $\pi-\pi$ interactions occurring between the two Pc ligands in lanthanide (Ln)-Pc complexes.[30] It is well-documented that all MPc_2 molecules show a strong IR band at ca. 1370 cm^{-1} which is a diagnostic band for the Pc π-radical (see Figure S3 and Table S3, Supporting Information).[31]

To characterize the electronic structure of $TbPc_2$ and $DyPc_2$, the redox potentials ($E_{1/2}$) were measured with DPV under following two conditions: (A) from −2.0 to +2.0 V and (B) from +2.0 to −2.0 V (see Figure S4 and Table S4, Supporting Information). Both conditions A and B gave quasi-five one-electron oxidation waves corresponding to the successive generation of cation/anion species and a poorly resolved second reduction wave at $E_{1/2}^{red2} \approx -1.35$ V in reference to the blank peak. The HOMO−LUMO gap (0.48 and 0.47 eV) of $TbPc_2$ and $DyPc_2$ are calculated from the difference between the first oxidation peak ($E_{1/2}^{ox}$) and first reduction peak ($E_{1/2}^{red1}$), respectively. These values are comparable with those reported for the $LnPc_2$ derivatives (ca. 0.4 eV)[32] and YPc_2 (0.46 eV).

Surface Morphologies of MPc_2 and MPc. Figure 2 illustrates typical STM images of the surface where a submonolayer of MPc_2 molecules (M = Tb^{3+}, Dy^{3+}, and Y^{3+}) was deposited on a Au(111) surface.[11c] On the Au(111) surface after deposition of $TbPc_2$ molecules, two types of molecules were observed, as shown in Figure 2a. The upper isolated molecule had four lobes, and the lower one had eight lobes. The Au(111) surface is shown in the inset of Figure 2a and the [1$\bar{1}$0] direction of the Au(111) surface is indicated by the arrow. The diagonal direction of the four-lobe molecule is parallel to the [1$\bar{1}$0] direction. For the eight-lobe molecule, we observed a node along this direction. The height of the molecules could be clearly measured in the cross-section views, which are shown in Figure 3. The four-lobe and the eight-lobe molecules had heights of 140 and 400 pm, respectively. These images were obtained for $TbPc_2$, but the shape and the nominal heights of the molecules were similar for all MPc_2 molecules (M = Tb^{3+}, Dy^{3+}, and Y^{3+}) except the ratio of the eight-lobed feature decreased in the order of YPc_2 > $TbPc_2$ > $DyPc_2$. In Figure 2b, a group of the isolated four-lobe molecules adsorbed on the terrace part of the substrate are shown. Some of the molecules had a dip in the center.

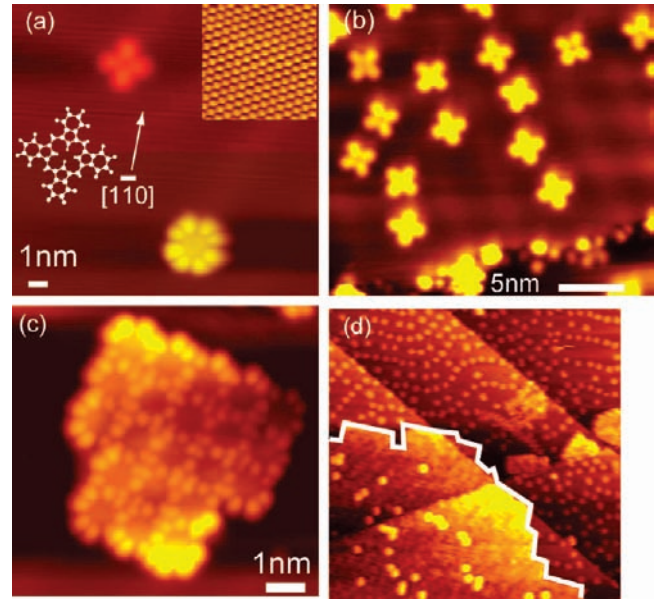

Figure 2. STM images of $TbPc_2$ and TbPc. (a) single molecules of TbPc (upper) and $TbPc_2$ (lower). An atomic image of the Au(111) is shown in the inset. The [1$\bar{1}$0] direction is marked by the arrow. Schematic models of the Pc plane of the observed TbPc and $TbPc_2$ molecules are superimposed. (b) TbPc molecules on the terrace part of the Au(111) surface (25 × 23 nm^2). (c) $TbPc_2$ film composed of 21 molecules (7.8 × 7.8 nm^2). (d) Coexisting $TbPc_2$ island and isolated TbPc molecules. The boundary of the former is highlighted by the white line in the image (area 80 × 80 nm^2).

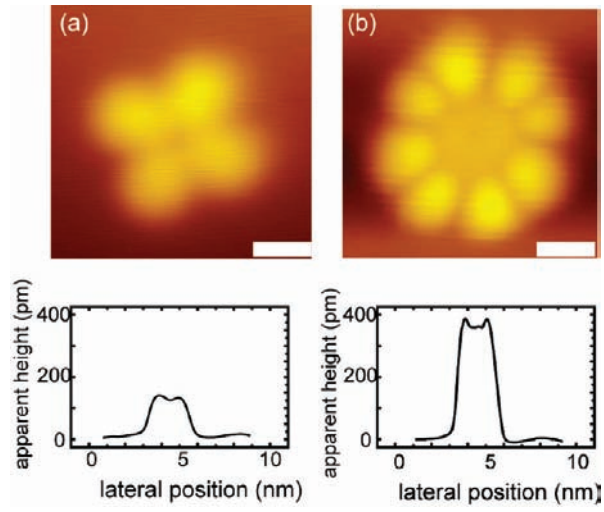

Figure 3. Topographic image and cross-sectional view of the (a) TbPc and (b) $TbPc_2$ molecules. Bars indicate 1 nm.

We observed the formation of islands of the $TbPc_2$ molecules, as shown in Figure 2c. The molecules formed a nearly square lattice, whose height (~400 pm) and shape (eight bright spots on the rim) are similar to the eight-lobe molecule in Figure 2a. Again similar islands are commonly observed for the three molecules. In Figure 2d, we observed the coexistence of square-lattice islands and isolated molecules, the former of which can be seen in the lower-left corner. The boundary is highlighted by a white line. It is difficult to estimate the ratio of the MPc and MPc_2 molecules because their hopping barriers seem to be significantly different. In addition, the MPc_2 molecules mainly

(28) Padilla, J.; Hatfield, W. E. *Synth. Met.* **1989**, *29*, F45–F50.
(29) Markovitsi, D.; Tran-Thi, T.-H.; Even, R.; Simon, J. *Chem. Phys. Lett.* **1987**, *137*, 107–112.
(30) Iwase, A.; Harnoode, C.; Kameda, Y. *J. Alloys Compd.* **1993**, *192*, 280–283.
(31) Kadish, K. M.; Moninot, G.; Hu, Y.; Dubois, D.; Ibnlfassi, A.; Barbe, M.; Guilard, R. *J. Am. Chem. Soc.,* **1993**, *115*, 8153–8166.
(32) Jiang, J.; Liu, R. C. W.; Mak, T. C. W.; Chan, T. W. D.; Ng, D. K. P. *Polyhedron* **1997**, *16*, 515–520.

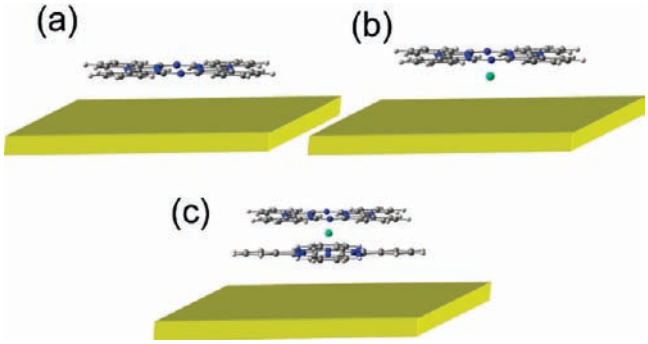

Figure 4. Schematic illustrations of the adsorption configurations of (a) Pc, (b) MPc, and (c) MPc_2 on the Au (111) substrate.

form islands, and MPc molecules are isolated on the terrace. A rough estimation of the ratio of the MPc_2 and MPc molecules from Figure 2b is 4:1.

First, we examined the four-lobe molecule. The measured height of ~140 pm is in the range of the previously reported heights of isolated molecules of CoPc,[15,33−35] FePc,[18] and metal-free Pc,[36] which have been observed at cryogenic temperature. In addition, they showed a cross-like shape in the topographic image, which is similar to the ones in Figure 2a. Thus, we think that the four-lobe molecule corresponds to either a MPc or a Pc molecule instead of a MPc_2 molecule. The MPc and Pc molecules might be formed by a cracking of the molecule MPc_2 in the sublimation process. The molecule shape and the bonding configuration of (a) Pc, (b) MPc, and (c) MPc_2 molecules are illustrated in Figure 4, and the four-lobe molecule should correspond either to (a) or (b). A model of the bonding configuration, which is expected to be similar for the Pc and MPc molecules, is superimposed in Figure 2a.

To determine the electronic structure of the MPc molecules, the valence state of the metal in the molecules must be determined. However, we could not isolate MPc (M = Tb^{3+}, Dy^{3+}, and Y^{3+}). Generally, neutral lanthanide (Ln^0) groups can easily be oxidized to the trivalent state (Ln^{3+}). Therefore, we believe that the metal ions in the MPc molecules on the Au(111) substrate are in a +3 oxidation state (M = Tb^{3+}, Dy^{3+}, and Y^{3+}). Thus, we attempted to determine whether the target four-lobe molecule was Pc or MPc. The reported image shape and the height for (a) and (b) are similar for a variety of the center atoms, which makes it difficult to distinguish the cases of (a) and (b). However they can be distinguished clearly by a conductance mapping method that will be discussed in later.

The MPc_2 molecule should have the bonding configuration shown in Figure 4c. As shown above, the upper Pc plane and the lower Pc plane are rotated ~45°. Thus, if we assume a similar bonding configuration between the lower Pc plane and the substrate (the diagonal direction is parallel to $[1\bar{1}0]$), the model should be the one schematically shown in Figure 2a (bright Pc corresponds to the upper Pc plane). The eight bright spots should be located on both sides of each benzene ring. A height value of ~400 pm is consistent with the size of the MPc_2 molecules determined by using X-ray analysis. The individual molecules in the terrace area appeared trapped along the hcp-fcc boundary of the herringbone structure.

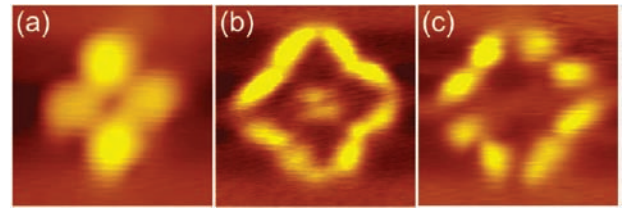

Figure 5. (a) Topographic image and conductance mapping of YPc molecule at sample bias voltages of (b) 0.8 and (c) −0.8 eV.

Composition Analysis of the M-Pc Films. To determine if the MPc_2 molecules crack during the evaporation process or if Pc molecules selectively evaporate leaving metal atoms in the boat, we studied the element concentration by using XPS on the powder samples prior to evaporation and on the deposited thin films, which were 2−4 nm thick. The XPS peaks were analyzed with a standard background subtraction, and the integrated areas were calculated with a calibration using atomic sensitivity factors.[37]

The data obtained on the $DyPc_2$ molecules showed that the ratio N:Dy was 100:4.0 prior to thermal deposition, and it was 100:7.0 in the film after the deposition. The ratio of atoms in the molecule is 100:6.2. The data suggests that the metal atoms are not left in the boat and consequently four-lobed features are not just Pc molecules. It was noted that the isolated molecules trapped at the boundary of the herringbone structure were dominated by four-lobe molecules. This might indicate a difference in the activation barrier for lateral diffusion of the four-lobe and the eight-lobe molecules. In other words, the four-lobe molecules have a higher barrier for lateral diffusion, since a metal ion protruding from a Pc ligand toward the Au surface should have a higher activation barrier for lateral hopping than the flat Pc rings of the MPc_2 molecules should.

d*I*/d*V* Mapping of the Four-lobed Molecule. Here we show that the conductance (d*I*/d*V*) mapping of the molecule can be used to distinguish between MPc and Pc molecules. An example of d*I*/d*V* mappings obtained for the four-lobe YPc are shown in Figure 5. Unlike the cross-like shape of the topographic image of Figure 5a, the d*I*/d*V* mapping at bias voltages of (b) 0.8 and (c) −0.8 V showed circular bright areas. In particular, we could distinguish eight bright spots for the negative sample bias. The bright areas are located on both sides of the benzene rings, the latter of which are highlighted in the topographic image. This type of d*I*/d*V* mapping, however, was obtained for approximately half of the isolated molecules. The rest of the molecules showed no significant features in the d*I*/d*V* mapping. We believe that the latter half corresponds to the Pc molecules, which have no metal atom at the center.

To determine if this is the case, we evaporated metal-free Pc on the Au(111) and measured the d*I*/d*V* mapping. The results are shown in Figure 6, and the d*I*/d*V* mapping of the Pc molecule barely showed any significant features. This can be confirmed by the STS spectra obtained on the ligand position (near the four lobes) for both molecules. Distinct features at $V = -0.9$ and 1.2 V were observed only for YPc. Similar peaks were observed for an isolated CoPc molecule at $V = -0.8$ and 1.1 V, which were attributed to HOMO-1 and LUMO orbitals.[35] These features were measured as strong peaks when the tip was

(33) Krgöer, J.; Jensen, H.; Néel, N.; Berndt, R. *Surf. Sci.* **2007**, *601*, 4180–4184.
(34) Takada, M.; Tada, H. *Chem. Phys. Lett.* **2004**, *392*, 265–269.
(35) Takada, M.; Tada, H. *Jpn. J. Appl. Phys. Part 1* **2005**, *44*, 5332–5335.
(36) Isshiki, H.; Zhang, Y. F.; Komeda, K. *J. Phys. Chem. C* Manuscript in preparation.
(37) Wagner, C. D.; Davis, L. E.; Zeller, M. V.; Taylor, J. A.; Raymond, R. M.; Gale, L. H. *Surf. Interface Anal.* **1981**, *3*, 211.

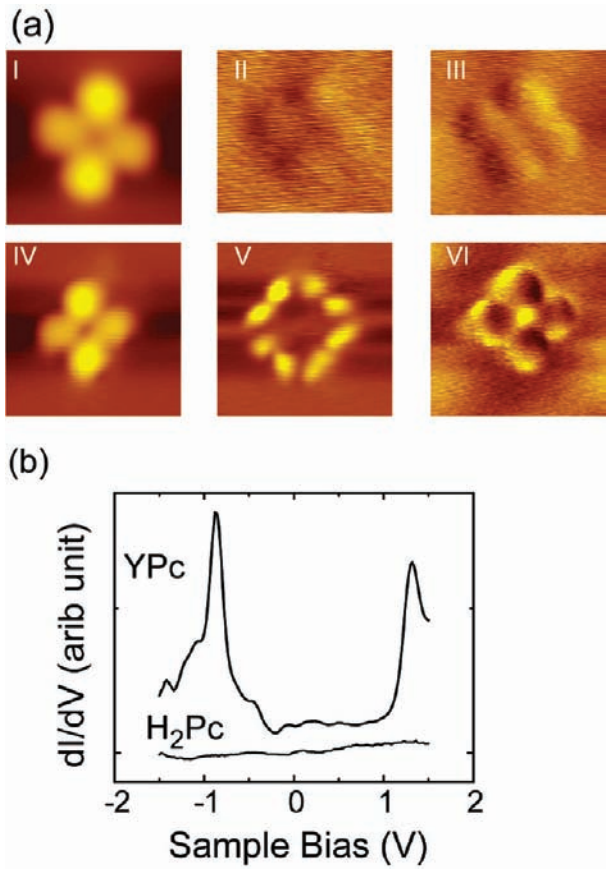

Figure 6. Conductance mapping of Pc and YPc: (a) I, II, and III (IV, V, and VI) correspond to the topographic image, dI/dV mapping at $V = -0.8$ eV, dI/dV at $V = -0.4$ eV for the Pc (YPc) molecule. (b) STS spectra of Pc and YPc measured at the center of the molecule.

positioned close to the benzene rings. In gas-phase ultraviolet photoemission spectroscopy, it was shown that the HOMO and HOMO-1 levels were not dependent on the central metal ions.[38] Thus, the features at $V = -0.9$ and 1.2 V observed for the YPc molecule were attributed to HOMO-1 and LUMO levels, both of which are distributed mainly around the benzene rings. However, in the same photoemission experiment, the HOMO feature was clearly observed for the metal-free Pc.[38] The absence of the features at $V = -0.9$ and 1.2 V for the metal-free Pc suggests that the center metal plays a role in the appearance of these peaks in the STS spectra, even though the HOMO and LUMO states exist in the metal free Pc.

The same phenomena were observed for the TbPc molecule, as shown in Figure 7. The conductance mapping at $V = -0.8$ V showed eight bright areas, which is similar to the one for the YPc in Figure 6a. In the STS spectrum, peaks were observed at $V = -0.9$, -0.5, and 1.2 V, which were not observed in the spectrum measured on the bare Au surface. The peaks are also similar to the ones observed for the YPc molecule, except for the clear feature at $V = -0.5$ V, which might be HOMO level. The STS peak of the HOMO level of CoPc on the Au(111) substrate has been reported to be at $V = -0.5$ V.[35]

With the conductance mapping at the energy levels close to HOMO-1 and LUMO, we can distinguish LnPc and metal-free Pc, both of which can be considered daughter molecules of the double-decker $LnPc_2$.

(38) Berkowitz, J. *J. Chem. Phys.* **1979**, *70*, 2819–2828.

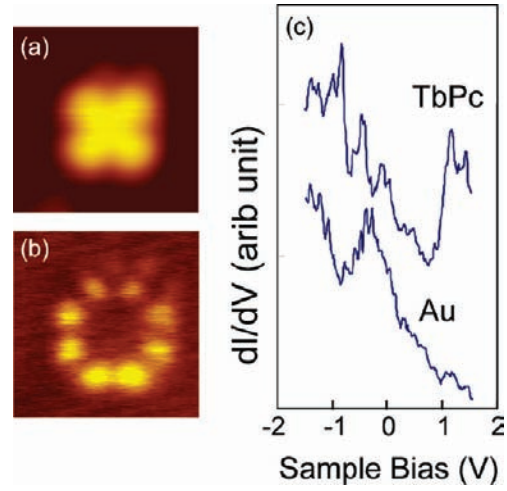

Figure 7. (a) Topographic image, (b) the conductance mapping at $V = -0.8$ eV, and (c) STS of the molecule TbPc. In the plot of STS, the data obtained on the bare Au substrate are superimposed.

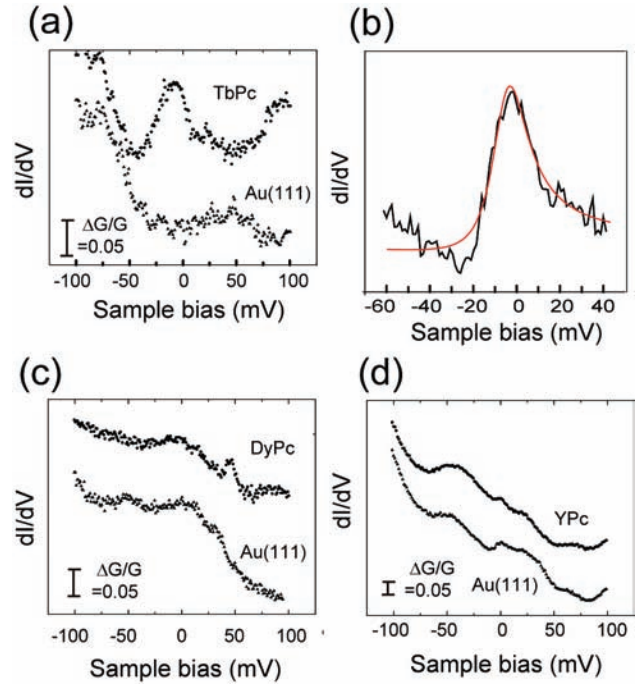

Figure 8. High-resolution STS spectra of (a) TbPc, (c) DyPb, and (d) YPc. The dI/dV data were obtained using the lock-in amplifier with a modulation voltage of 4 mV. All were obtained by placing the tip at the center of the molecules. (b) Fitting of the spectrum of TbPc with a Fano-shaped function, which is described in the main text. Smooth red curve is the result of the best fitting.

STS Measurements Near the Fermi Level. High resolution STS measurements near the Fermi level were performed on the four-lobed molecules MPc and the eight-lobed molecules MPc_2 ($M = Tb^{3+}$, Dy^{3+}, and Y^{3+}). The dI/dV spectra obtained on the bare Au(111) surface and on the center of the TbPc molecule are compared in Figure 8a. A sharp peak near the Fermi level with a width of ~20 meV was observed. The appearance of the peak was position-sensitive, and it disappeared when the tip was shifted from the center of the molecule. These features are similar to those previously reported for Kondo peaks observed in the spectra of isolated magnetic atoms[16] and molecules containing magnetic atoms.[13−15,39] A magnification of spectrum around the Fermi level is shown in Figure 8b. It

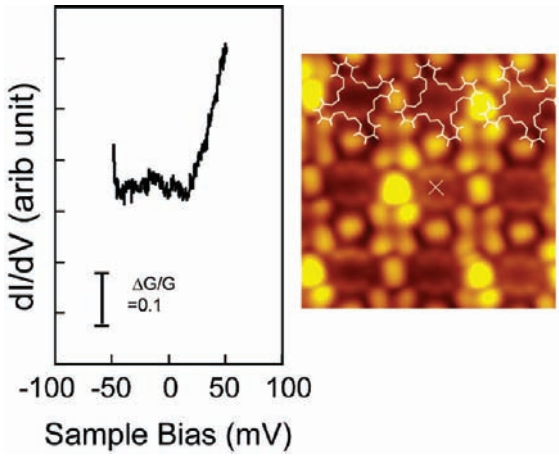

Figure 9. High resolution STS spectrum of $TbPc_2$ (conditions are same as Figure. 8). A topographic image of the $TbPc_2$ monolayer-film is shown with a tentative model of the configuration of the top-layer Pc and the position of the STS measurement (×).

has a Lorentzian-like peak shape with a slower decay in the right-hand side. The Kondo feature had a Fano shape and was analyzed using the following formula:[40−42]

$$\frac{dI(V)}{dV} = A\frac{(\varepsilon + q)^2}{1 + \varepsilon^2} + B, \quad \varepsilon = \frac{eV + \varepsilon_0}{\Gamma}$$

where A is an amplitude, B is a background, ε_0 is the energy shift of the resonance from the Fermi level, and Γ is the half width of the resonance (2Γ is equal to the full-width half-maximum). The curve was fitted with $\Gamma \approx 11$ mV and $q \approx 4.5$. This result gave a Kondo temperature (T_K) of ~250 K, which is similar to those reported for CoPc ($T_K \approx 208$ K)[15] and FePc ($T_K \approx 360$ K).[18] The q parameter corresponds to the coupling of the tip and the magnetic impurity. A low value of q implies a strong coupling between the tip and the conduction electron of the substrate, and a high value of q corresponds to a strong coupling between the tip and the magnetic impurity. The former gives a symmetric dip in the spectrum, whereas the latter gives a Lorentzian shape. The peak shape observed in this experiment corresponds to the latter case with $q \approx 4.5$, implying a strong coupling between the tip and the Tb ions and a weak coupling between the substrate and the Tb 4f orbital.

In the dI/dV spectra of DyPc and YPc shown in Figures 8c and d, no sharp features at the Femi level were observed, meaning that these two molecules show no Kondo features. Though small peaks were observed in the spectra, they are commonly observed both for the molecules and Au due to the electronic structure of the tip.

The dI/dV spectra obtained of a film of the $TbPc_2$ molecule is shown in Figure 9, in which the topographic image of the film and a proposed model of the molecule arrangement are shown. The spectra were obtained at the position marked by × in Figure 9. The dI/dV showed no obvious sharp peak at the Fermi level.

We consider the mechanism for the appearance/absence of the Kondo feature for the four-lobe species. First, let us note that $S = 0$, 5/2, and 3 for Y^{3+}, Dy^{3+}, and Tb^{3+}, respectively. The absence of the Kondo peak for YPc can be explained by the absence of a spin for Y^{3+}. Though both Dy^{3+} and Tb^{3+} have spins, the Kondo peak was observed only for the latter case. This should be analyzed with considering the exchange coupling parameter J, which is mainly for the coupling between

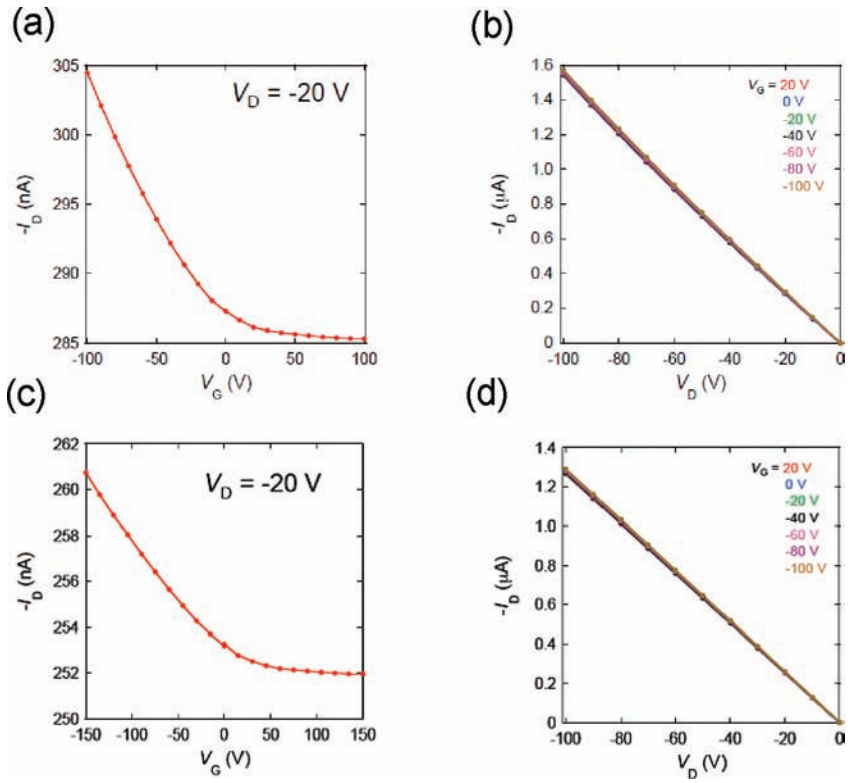

Figure 10. Tb-Pc p-channel OFETs devices: (a) transfer and (b) output characteristics of the bottom-contact device; (c) transfer and (d) output characteristics of the top-contact device.

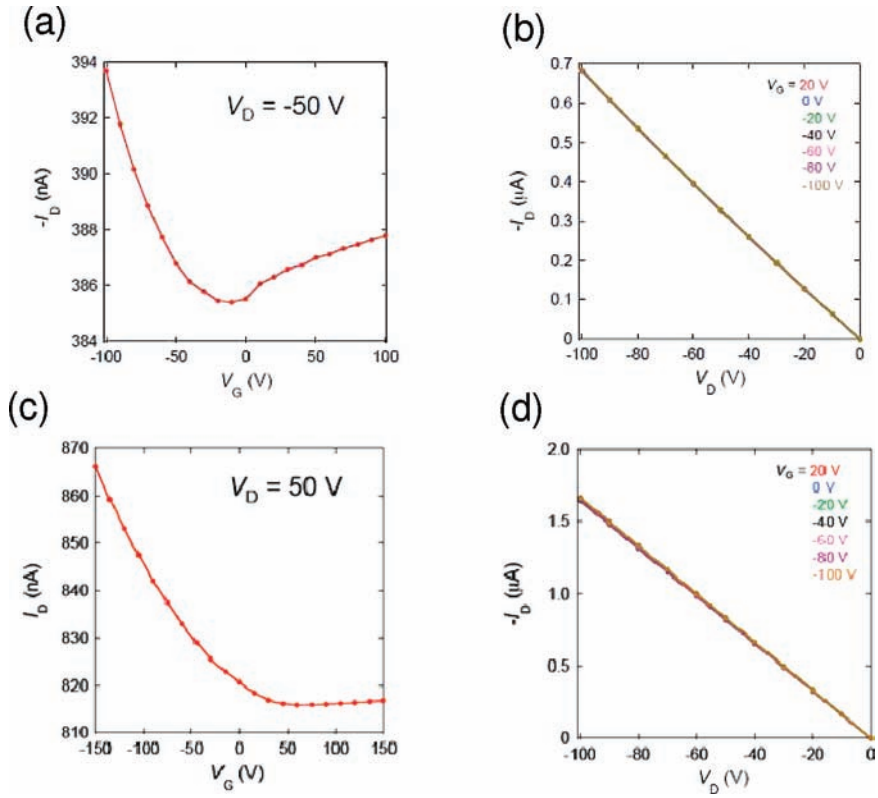

Figure 11. Dy-Pc ambipolar-channel OFETs devices: (a) transfer and (b) output characteristics of the bottom-contact device; (c) transfer and (d) output characteristics of the top-contact device.

Tb 4f and the conduction electron. T_K is approximated by using the following formula:[43]

$$k_B T_K \sim D \exp\left(-\frac{1}{2}\rho_0 J\right)$$

where k_B is Boltzmann's constant, ρ_0 is the density of state at the Fermi level, and D is the half width of the conduction band. Zhao et al. argued that, in considering the Kondo feature in a molecular system, J should be divided into two components that are sensitive (J_d) and not-sensitive (J_0) to a substrate-magnetic impurity distance of d.[44] In other words, J_d is mainly determined by d, and J_0 is derived from the coupling between the ligand orbitals and Tb 4f electrons. The averaged height of the four-lobe molecules of TbPc and DyPc were with our experimental error of 10 pm. Thus, we assumed that J_d was similar for both cases. On the other hand, there should be a large energy difference between sublevels of Tb compared to those of Dy, which have been calculated by Ishikawa et al.[9] The energy difference between the ±6 ground state and the second stable ±5 state of $TbPc_2$ was larger than 400 cm^{-1}, whereas the difference between the ±13/2 and ±11/2 states of $DyPc_2$ has been calculated to be less than 50 cm^{-1}. The sublevel splitting is, at least partially, determined by J_0. Though these calculations involved $TbPc_2$ and $DyPc_2$, we believe that TbPc and DyPc have similar electronic configurations. The energy diagram suggests that the J_0 of TbPc is higher than that of DyPc. Since the total J is the sum of J_0 and J_d, a smaller J_0 causes a lower Kondo temperature. Furthermore, when T_K is lower than the sample temperature (~4.7 K), a Kondo peak should not be observed. We feel that this is the reason for the presence and absence of the Kondo peaks for the TbPc and DyPc molecules, respectively. The actual energy diagram of the sublevels of TbPc and DyPc are not clear. Further studies are necessary to determine the relationship between energy gap of the sublevels and the Kondo effect.

Field-Effect Transistor Properties of Tb- and Dy-Pc Thin Films. Top- and bottom-contact device structures are shown in Figure S5, Supporting Information. Typical transfer and output plots for Tb-Pc based FET devices are shown in Figure 10a,b (bottom contact) and 10c,d (top contact). Figure 10a and c show plots of the drain current (I_D) as a function of the gate voltage (V_G; transfer characteristic) with an applied drain-source voltage (V_D) of −20 V at ambient temperature. In the negative voltage region, I_D decreased with an increase in V_G. In other words, p-type semiconductor behavior was observed.

The bottom- and top-contact Tb-Pc based devices both exhibited p-channel behavior with a hole mobility (μ_H) of 4.0 × 10^{-4} cm^2 V^{-1} s^{-1} in a V_G range of −100 to 100 V and μ_H = 1.0 × 10^{-4} cm^2 V^{-1} s^{-1} in a V_G range of −150 to 150 V, respectively. The simultaneously measured gate leakage current was negligibly small for all prepared devices. We note that the current is induced only at the bottom surface of the semiconductor film by the electric field. Since the rest of the 200 nm thick film has sheet conductivity in the range of 1−10 S, only 4−7% of the total current is modulated. Thus, $I_{on}/I_{off} \approx 1.04-1.07$.

(39) Iancu, V.; Deshpande, A.; Hla, S.-W. *Phys. Rev. Lett.* **2006**, *97*, 266603–266604.
(40) Fano, U. *Phys. Rev.* **1961**, *124*, 1866–1878.
(41) Ujsaghy, O.; Kroha, J.; Szunyogh, L.; Zawadowski, A. *Phys. Rev. Lett.* **2000**, *85*, 2557–2560.
(42) Merino, J.; Gunnarsson, O. *Phys. Rev. B* **2004**, *69*, 115404–10.
(43) Hewson, A. C. *The Kondo Problem to Heavy Fermions*; Cambridge University Press: Cambridge, 1993.
(44) Zhao, A. D.; Hu, Z. P.; Wang, B.; Xiao, X. D.; Yang, J. L.; Hou, J. G. *J. Chem. Phys.* **2008**, *128*, 234705–234706.

Typical transfer and output plots for the Dy-Pc based OFETs are shown in Figure 11a,b (bottom contact) and 11c,d (top contact). Interestingly, the Dy-Pc based devices were ambipolar under ambient conditions. The highly delocalized π system of sandwich phthlocyaninato rare earth(III) complexes exhibit great potentials as ambipolar semiconductors for OFETs as revealed by the pioneering work of Simon and co-workers.[24d]

The bottom-contact device exhibited both μ_e (1.1×10^{-5} cm^2 V^{-1} s^{-1}) and μ_H (1.2×10^{-4} cm^2 V^{-1} s^{-1}) and an I_{on}/I_{off} of 1.03 in a V_G range of -100 to 100 V, as shown in Figures 11a,b. Although the top-contact devices had similar μ_H (1.0×10^{-4} cm^2 V^{-1} s^{-1}), the values of μ_e (3.0×10^{-6} cm^2 V^{-1} s^{-1}) were 1/10 of those of the bottom-contact devices ($I_{on}/I_{off} = 1.04$ in a V_G range of -150 to 150 V; Figures 11c,d). Thus, the apparent μ_e of the bottom-contact devices was higher than that of the top-contact ones.

The values of μ_e for these devices are thought to be due to several factors, such as the percentage of $LnPc_2$, LnPc, and Pc in the samples, HOMO and LUMO levels of these samples, work function of the metal contact, the energy gap of the samples, intermolecular π-orbital overlap in the films, grain size of films, effect of oxygen[25f] and water molecules, etc. Although the present unoptimized mobilities are moderate, to the best of our knowledge this is first example of air-stable, Ln(III)-Pc molecules.

Conclusions

We investigated the characteristics of the lanthanide-phthalocyanine molecules $LnPc_2$ and LnPc (Ln = Tb^{3+}, Dy^{3+}, and Y^{3+}) deposited on a Au(111) surface. Both molecules were shown to coexist on the Au(111) surface on the basis of height profiles, XPS, and d*I*/d*V* mapping. A Kondo peak was observed only for TbPc. By fitting the STS signal, we determined that the energy width of the feature corresponded to a Kondo temperature (T_K) of $\sim$250 K, which is similar to those for the 3*d* metal complexes CoPc[15] and FePc.[18] The Kondo effect was not observed with the molecules of DyPc and YPc. We believe that the splitting energy of sublevels of these molecules in a crystal field are critical for understanding the Kondo effect, and the relation between T_K and the blocking temperature (T_B) must be discussed further.

To investigate the electronic structure of Ln(III)-Pc molecules, we fabricated a top-contact and bottom-contact thin-film OFETs device. We found that the Tb-Pc based devices showed *p*-channel characteristics. On the other hand, Dy-Pc based devices exhibited both hole and electron transport properties (ambipolar-channel characteristics).[24d] To the best of our knowledge, this was first observation of electron transport properties in Ln(III)-Pc molecules, providing a good starting point for designing complexes with electron transport properties for OFETs. The use of the mixed MPc device makes it possible to study the processes associated with film formation and diffusion in two or three dimensions. The relationship between electronic transport properties and film/electronic structures are under investigation. Understanding and being able to measure the magnetic coupling/electronic transport properties of a single molecule of rare-earth metal(III)-Pc_2 molecules is expected to play a key role in the design of spintronic devices.

Acknowledgment. This work was financially supported by a Grant-in-Aid for Scientific Research (S) (Grant No. 20225003) from the Ministry of Education, Culture, Sports, Science, and Technology, Japan.

Supporting Information Available: Crystal structures (CIF format), spectral, and voltammetric data for MPc_2 (M = Tb^{3+}, Dy^{3+}, and Y^{3+}). This material is available free of charge via the Internet at http://pubs.acs.org.

JA902349T